Experimental implementation of a quantum random-walk search algorithm using strongly dipolar coupled spins

Dawei Lu,[1] Jing Zhu,[1,2] Ping Zou,[3] Xinhua Peng,[1] Yihua Yu,[2] Shanmin Zhang,[2] Qun Chen,[2] and Jiangfeng Du[1,*]

[1]*Hefei National Laboratory for Physical Sciences at Microscale and Department of Modern Physics, University of Science and Technology of China, Hefei, Anhui 230026, People's Republic of China*

[2]*Department of Physics & Shanghai Key Laboratory for Magnetic Resonance, East China Normal University, Shanghai 200062, People's Republic of China*

[3]*Laboratory of Quantum Information Technology, International Centre for Materials Physics and SPTE, South China Normal University, Guangzhou 510006, People's Republic of China*

(Received 20 October 2009; published 9 February 2010)

An important quantum search algorithm based on the quantum random walk performs an oracle search on a database of N items with $O(\sqrt{phN})$ calls, yielding a speedup similar to the Grover quantum search algorithm. The algorithm was implemented on a quantum information processor of three-qubit liquid-crystal nuclear magnetic resonance (NMR) in the case of finding 1 out of 4, and the diagonal elements' tomography of all the final density matrices was completed with comprehensible one-dimensional NMR spectra. The experimental results agree well with the theoretical predictions.

DOI: 10.1103/PhysRevA.81.022308 PACS number(s): 03.67.Lx, 05.40.Fb, 76.60.−k

I. INTRODUCTION

Quantum computation has attracted much attention for the past decade as it is believed that quantum computers can efficiently solve problems that are intractable to classical computers. The computation tasks are rendered by algorithms. Since Shor's remarkable factoring algorithm [1], many quantum algorithms have been proposed. The algorithms presented earlier have been mainly based on the quantum Fourier transform [1] and Grover's search algorithm [2]. Later, two alternative trends entered into the field: the adiabatic quantum algorithms [3] and quantum random walk [4–12]. In this paper, we focus on the quantum-walk-based search algorithm.

Since the classical random walk is a useful tool for developing classical algorithms, the quantum random walk has been introduced as a potential method to formulate quantum algorithms. There are two distinct models, the continuous-time model and discrete-time model. The continuous-time model defines a Hamiltonian that acts continuously on the system to drive the quantum random walk. The discrete-time model requires an extra coin register and defines a two-step procedure consisting of a quantum coin flip followed by a coin-controlled walk step. Investigations show that quantum random walks have features that are notably different from their classical counterparts [4,5]. These features may be used for designing quantum algorithms. Some relevant algorithms have been discovered with remarkable speedup over classical computation [8,13]. The quantum search algorithm based on the quantum random walk proposed by Shenvi, Kempe, and Whaley (the SKW algorithm) [13] is one of the novel algorithms for performing an oracle search on a database of N items with $O(\sqrt{phN})$ calls, where N is the size of the search space. Despite a speedup similar to Grover's quantum search algorithm, the SKW algorithm is important because there are situations when the diffusion step of Grover's algorithm cannot be implemented efficiently. Various optimizations and improvements of the SKW algorithm have also been proposed in recent years [14–18], which reduce the complexity and increase the search capability to a certain extent.

Some experiments involving quantum random walk have been implemented in various physical systems under both continuous- and discrete-time conditions [19–22], but no experiments about the algorithms based on quantum random walk have been reported. In this paper, we experimentally demonstrate the 1 out of 4 case of the SKW algorithm [13] and show its superiority over classical algorithms. The experiments are performed on a quantum-information processor of liquid-crystal nuclear magnetic resonance, with a strongly dipolar coupled Hamiltonian [23–25]. More details are described in Sec. III.

II. ALGORITHM

First we give an overview of the original algorithm. Consider the following unstructured search problem: given a function $f(x)$, $f(x) = 1$ if $x = a$; otherwise $f(x) = 0$. The goal is to find a, where $0 \leqslant a \leqslant 2^n - 1$. It is equivalent to search for a single marked node among the $N = 2^n$ nodes on the n cube.

The discrete-time random walk can be described by the repeated application of a unitary evolution operator U. The operator U can be divided into two parts, $U = SC$, where S is a permutation matrix, which performs a controlled shift based on the state of the coin space, and C is a unitary matrix corresponding to "flipping" the quantum coin. To search for the node, the SKW algorithm introduces an oracle whose function is determined by the coin operator. The oracle acts by applying a marking coin C_1 to the marked node and the original coin C_0 to the unmarked nodes. This new coin operator is named C'. Then the perturbed unitary evolution operator U' is given by $U' = SC'$ (see Fig. 1). After applying U' for $t_f = \frac{\pi}{2}\sqrt{2^n}$ times, we gain the marked state with probability $\frac{1}{2} - O(n)$ by measurement.

When $n = 2$, three qubits are needed to demonstrate the algorithm. One qubit is used as the "coin" (referred to as the

*djf@ustc.edu.cn

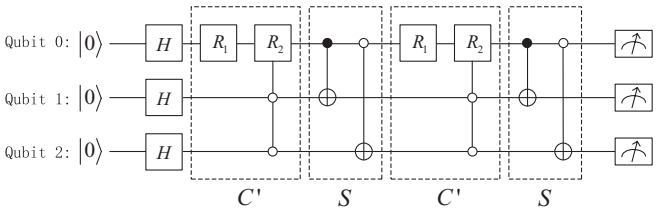

FIG. 1. Quantum network for the algorithm of 1 out of 4 searching, with the target state being $|00\rangle_{12}$. Qubit 0 is the "coin qubit," while qubit 1 and 2 are "database qubits." The Hadamard gates are applied to produce an equal superposition over all the computational bases. The solid circle represents a 1-control gate whereas the open circle represents the opposite. The purpose of C' is to implement $C_1 = R_x^0(\pi/2)$ (rotating qubit 0 around the x axis by angle $\frac{\pi}{2}$) when the "database" is $|00\rangle_{12}$ and $C_0 = R_x^0(3\pi/2)$ otherwise. It is equivalent to being replaced by $R_1 = R_x^0(3\pi/2)$ and $R_2 = R_x^0(-\pi)$. The two controlled-NOT gates invert qubit 1 if qubit 0 is $|1\rangle_0$ and invert qubit 2 if qubit 0 is $|0\rangle_0$, respectively. The measurement is all the populations' diagonal-element reconstruction. Similar circuits can be obtained in a straightforward manner for other target states. For instance, if the goal is $|10\rangle_{12}$, we need only change the controlled condition of the three-body-interaction gate to state $|10\rangle_{12}$.

"coin qubit," labeled by qubit 0), whereas the other two are used as the database (referred to as the "database qubits," labeled by qubits 1 and 2). The target state is $|\tau\sigma\rangle_{12} = |\tau\rangle_1 \otimes |\sigma\rangle_2$ ($\tau, \sigma = 0, 1$) out of the four computational bases $|00\rangle_{12}$, $|01\rangle_{12}$, $|10\rangle_{12}$, and $|11\rangle_{12}$. The 1 out of 4 algorithm is implemented as the network shown in Fig. 1. Suppose the initial state is $|000\rangle$.

(i) Prepare the state

$$|\psi_i\rangle = \frac{|0\rangle_0 + |1\rangle_0}{\sqrt{2}} \otimes \frac{|0\rangle_1 + |1\rangle_1}{\sqrt{2}} \otimes \frac{|0\rangle_2 + |1\rangle_2}{\sqrt{2}}, \quad (1)$$

which is an exactly equal superposition over all the computational bases. It is simple to do this by applying a Hadamard operation to every qubit.

(ii) Perform the unitary operation on the coin qubit depending on the state of database qubits, namely, $C_1 = R_x^0(\pi/2) = e^{-i\pi\sigma_x/4}$ if the database qubits are on the target state $|\tau\sigma\rangle_{12}$, and $C_0 = R_x^0(3\pi/2) = e^{-i3\pi\sigma_x/4}$ otherwise. (In Fig. 1, this controlled operation is simplified through $R_1 = R_x^0(3\pi/2) = e^{-i3\pi\sigma_x/4}$ and $R_2 = R_x^0(-\pi) = e^{i\pi\sigma_x/2}$, equivalently.) Therefore, the whole coin operation is

$$C' = C_0 \otimes (E_{12} - |\tau\sigma\rangle_{12\,12}\langle\tau\sigma|) + C_1 \otimes |\tau\sigma\rangle_{12\,12}\langle\tau\sigma|, \quad (2)$$

where E_{12} is the identity operator on the database qubits. Then the database qubits undergo the shift operation S conditioned on the state of the coin qubit:

$$\begin{aligned} |0\rangle_0|00\rangle_{12} &\Longleftrightarrow |0\rangle_0|01\rangle_{12}, \\ |0\rangle_0|10\rangle_{12} &\Longleftrightarrow |0\rangle_0|11\rangle_{12}, \\ |1\rangle_0|00\rangle_{12} &\Longleftrightarrow |1\rangle_0|01\rangle_{12}, \\ |1\rangle_0|01\rangle_{12} &\Longleftrightarrow |1\rangle_0|11\rangle_{12}. \end{aligned} \quad (3)$$

(iii) Repeat step (ii) twice to reach the final state:

$$|\psi_f\rangle = (SC')^2|\psi_i\rangle. \quad (4)$$

(iv) Measure the diagonal elements of the final density matrix to obtain the populations of the database qubits. For example, in the case of finding $|00\rangle_{12}$, we can calculate that the probabilities of $|00\rangle_{12}$, $|01\rangle_{12}$, $|10\rangle_{12}$, and $|11\rangle_{12}$ are 0.5, 0.25, 0.25, and 0, respectively, after tracing qubit 0 out.

For other target states, similar circuits can easily be given with the controlled condition changed. The theoretical results have an analogy with the aforementioned algorithm.

III. EXPERIMENTAL IMPLEMENTATION

A. System

To implement the algorithm we used the three ^{1}H spins in a sample of 1-bromo-2,3-dichlorobenzene oriented in liquid-crystal solvent (ZLI-1132). All experiments were conducted on a Bruker Avance 500-MHz spectrometer at room temperature. The molecular structure is shown in Fig. 2(a). The internal Hamiltonian of this system can be described as

$$\mathcal{H} = \sum_{j=1}^{3} 2\pi\nu_j I_z^j + \sum_{j,k,j<k\leqslant 3} 2\pi J_{jk}\left(I_x^j I_x^k + I_y^j I_y^k + I_z^j I_z^k\right) + \sum_{j,k,j<k\leqslant 3} 2\pi D_{jk}\left(2I_z^j I_z^k - I_x^j I_x^k - I_y^j I_y^k\right), \quad (5)$$

where ν_j is the resonance frequency of the jth spin, and D_{jk} and J_{jk} are the dipolar coupling strengths and scalar coupling strengths between spins j and k, respectively. In the experiment, weak J couplings are assumed. The sums are restricted to the spins within one molecule. Since there exist nondiagonal elements in the Hamiltonian, the eigenstates are not Zeeman product states but linear combinations of them, and the eigenbasis is no longer the computational basis. We still use the computational basis to store and read information, while using the transformation matrix between the computational basis and eigenbasis for more obvious and

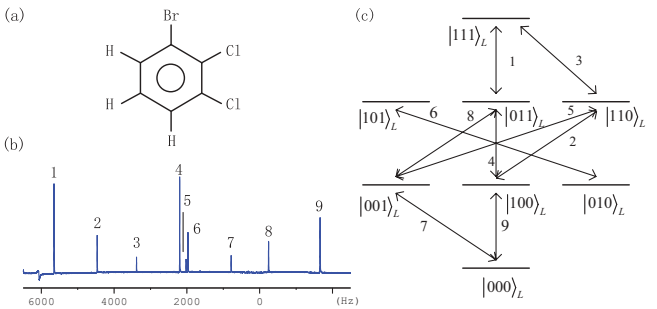

FIG. 2. (Color online) (a) Molecular structure of 1-bromo-2,3-dichlorobenzene in which the three protons form a three-qubit system. (b) Spectrum of the thermal equilibrium state followed by a $\pi/2$ hard pulse. All the observable transitions are labeled according to descending orders of the frequencies. (c) Diagram of corresponding transitions in the eigenbasis. Only nine transitions are assigned. Lines 1 and 9, 2 and 8, and 3 and 7 express the transitions of qubits 1, 2, and 3 in the H_L picture, respectively.

TABLE I. Parameters for fitting the spectrum of 1-bromo-2,3-dichlorobenzene (hertz). The diagonal elements are chemical shifts of the three protons, the upper-right off-diagonal elements are dipolar coupling strengths, and the lower-left ones are scalar coupling strengths.

	H_1	H_2	H_3
H_1	1945.5	−1633.3	−1341.7
H_2	8	2094.8	−339.35
H_3	8	1.4	2147.2

convenient reading of nuclear magnatic resonance (NMR) spectra.

The spectrum of the thermal equilibrium state $\rho_{th} = \sum_{i=1}^{3} \sigma_z^i$ followed by a $\pi/2$ hard pulse is shown in Fig. 2(b). Using some initially guessed parameters to assume the molecular geometry, we iteratively fit the calculated and observed spectra through the parameters' perturbation [26]. All the calculated values are listed in Table I: H_2, H_1, and H_3 are used as coin qubit 0 and database qubits 1 and 2 in the experiment, respectively.

The eigenstates $|\phi_i\rangle$ (where i is an integer and $1 \leqslant i \leqslant 8$) and eigenvalues E_i in this system can be solved easily once the Hamiltonian is confirmed. The intensity I_{ij} of all possible transitions between $|\phi_i\rangle$ and $|\phi_j\rangle$ can be obtained since

$$I_{ij} \propto \langle \phi_i | I^+ | \phi_j \rangle^2, \tag{6}$$

where $I^+ = \sum_{k=1}^{3} (I_x^k + i I_y^k)$. The corresponding transition frequencies are

$$\omega_{ij} = E_i - E_j. \tag{7}$$

In this system there are 15 possible transitions, for which 6 of them are less than 1% in amplitude compared to transition 1. In Fig. 2(b) we just focus on the nine observable transitions as signal-to-noise ratio issues.

B. Population measurement

With the system Hamiltonian confirmed, we consider the procedure of diagonalizing the Hamiltonian. It is not difficult to find a feasible unitary matrix U to equalize

$$H_L = U H_S U^\dagger, \tag{8}$$

where H_S is the system Hamiltonian and H_L is a diagonal Hamiltonian (i.e., the Hamiltonian in the eigenbasis). Particularly for the aforementioned system Hamiltonian, since U is not unique, we chose the transformation U to be

$$\begin{pmatrix} 1 & 0 & 0 & 0 & 0 & 0 & 0 & 0 \\ 0 & 0.801 & 0.512 & 0 & -0.303 & 0 & 0 & 0 \\ 0 & 0.375 & -0.823 & 0 & -0.420 & 0 & 0 & 0 \\ 0 & 0 & 0 & 0.810 & 0 & 0.126 & 0.559 & 0 \\ 0 & -0.467 & 0.223 & 0 & -0.856 & 0 & 0 & 0 \\ 0 & 0 & 0 & 0.458 & 0 & -0.730 & -0.508 & 0 \\ 0 & 0 & 0 & 0.344 & 0 & 0.672 & -0.656 & 0 \\ 0 & 0 & 0 & 0 & 0 & 0 & 0 & 1 \end{pmatrix}.$$

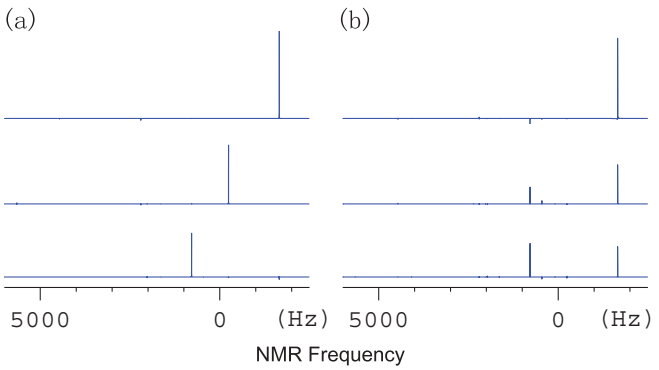

FIG. 3. (Color online) Simulation of the PPS's observation. (a) Spectra with the readout pulses $U R_1^y(\pi/2)$, $U R_2^y(\pi/2) R_3^y(\pi)$, and $U R_3^y(\pi/2)$; (b) spectra with the traditional readout pulses $R_1^y(\pi/2)$, $R_2^y(\pi/2)$, and $R_3^y(\pi/2)$. We can see that the spectra in part (a) are more comprehensible than those of part (b).

Through this labeling scheme all the transitions are between two eigenstates from $|000\rangle_L$ to $|111\rangle_L$ with $|000\rangle_L = |000\rangle_S$, $|111\rangle_L = |111\rangle_S$, where the subscripts L and S represent the eigenbasis and computational basis. The nine observable transitions in the thermal equilibrium spectrum are marked in the transition diagram [Fig. 2(c)].

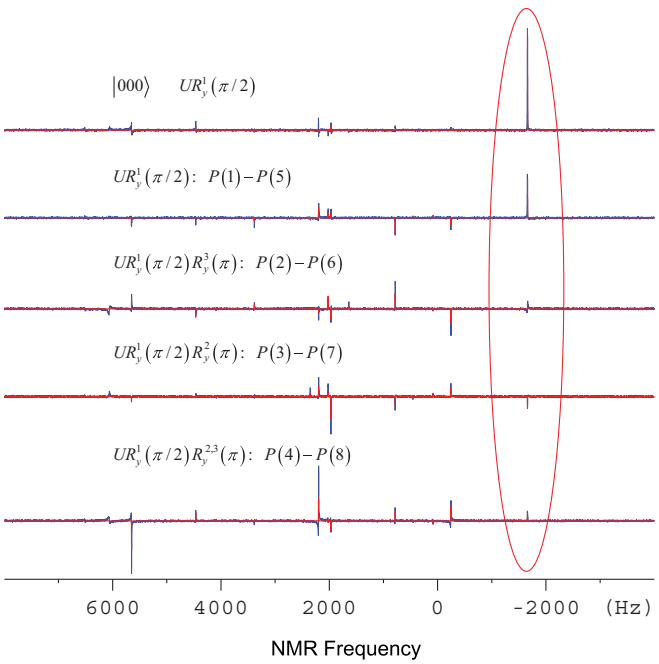

FIG. 4. (Color online) One-dimensional NMR spectra for measuring the diagonal elements of spin 1. The blue spectra (thick line) are the experimental results, while the red spectra (thin line) are the results by simulation. As shown in Table. II, we just concentrate on transition 9 (marked by the ellipse) to read out $P(1) - P(5)$, $P(2) - P(6)$, $P(3) - P(7)$, and $P(4) - P(8)$, with the four operators listed in the figure. The top spectrum is the observation of the PPS $|000\rangle$, which is used as the benchmark. The theoretical values of the four population subtractions are 0.375, 0, −0.125, and 0.125, while the experimental results are 0.383, 0.050, −0.061, and 0.093.

TABLE II. Readout pulses and corresponding values of $P(i) - P(j)$. The results are shown for transitions 9, 8, and 7. Combined with the normalized condition $\sum_{i=1}^{8} P(i) = 1$, all the diagonal elements can be solved.

Spin 1	$UR_y^1(\pi/2)$	$UR_y^1(\pi/2)\,R_y^2(\pi)$	$UR_y^1(\pi/2)\,R_y^3(\pi)$	$UR_y^1(\pi/2)\,R_y^{2,3}(\pi)$
Transition 9	$P(1) - P(5)$	$P(3) - P(7)$	$P(2) - P(6)$	$P(4) - P(8)$
Spin 2	$UR_y^2(\pi/2)$	$UR_y^2(\pi/2)\,R_y^1(\pi)$	$UR_y^2(\pi/2)\,R_y^3(\pi)$	$UR_y^2(\pi/2)\,R_y^{1,3}(\pi)$
Transition 8	$P(2) - P(4)$	$P(6) - P(8)$	$P(1) - P(3)$	$P(5) - P(7)$
Spin 3	$UR_y^3(\pi/2)$	$UR_y^3(\pi/2)\,R_y^1(\pi)$	$UR_y^3(\pi/2)\,R_y^2(\pi)$	$UR_y^3(\pi/2)\,R_y^{1,2}(\pi)$
Transition 7	$P(1) - P(2)$	$P(5) - P(6)$	$P(3) - P(4)$	$P(7) - P(8)$

Without loss of generality, we focused on the three rightmost transitions (7, 8, and 9), considering a simple case for which ρ_S is a pure state $(|000\rangle\langle 000|)_S$. In the isotropic weak-coupling liquid system, if the transition of qubit 1 is excited [a selective pulse $R_y^1(\pi/2)$ is enough], a single peak can be obtained in the spectrum. This is a universal way to test the created pseudo-pure state (PPS) in liquid-state NMR. However, in the liquid-crystal system, a single qubit rotation leads not to a single peak but to a combination of some relative peaks [see Fig. 3(b)]. The complicated spectrum is obviously not convenient to read out the information of the density matrix. A straightforward idea to solve the problem is to use the eigenbasis where the Hamiltonian is diagonal. From Eq. (8) we can clearly see that adding the pulse from implementing transformation matrix U after the readout pulse in the sequence is suitable. Figure 3(b) shows the spectra of $(|000\rangle\langle 000|)_S$ with three readout pulses $UR_1^y(\pi/2)$, $UR_2^y(\pi/2)R_3^y(\pi)$, and $UR_3^y(\pi/2)$. The second pulse needs an $R_3^y(\pi)$ rotation because transition 8 represents $|001\rangle_L \rightarrow |011\rangle_L$, not $|000\rangle_L \rightarrow |010\rangle_L$. The simulating spectra accord well with the expected results, similarly to the liquid system.

For reading out the diagonal elements of a general density matrix ρ_S, the preceding method is still effective. Defining the populations of $(|000\rangle\langle 000|)_S$ to $(|111\rangle\langle 111|)_S$ are $P(1)$ to $P(8)$; $UR_1^y(\pi/2)$ excites the transitions $|000\rangle_L \rightarrow |100\rangle_L$ and $|100\rangle_L \rightarrow |000\rangle_L$, displayed in transition 9. Through this transition, we can obtain the value of $P(1) - P(5)$. Table II shows all the available values of $P(i) - P(j)$ through different readout pulses. Combined with the normalization condition $\sum_{i=1}^{8} P(i) = 1$, all eight population values can be

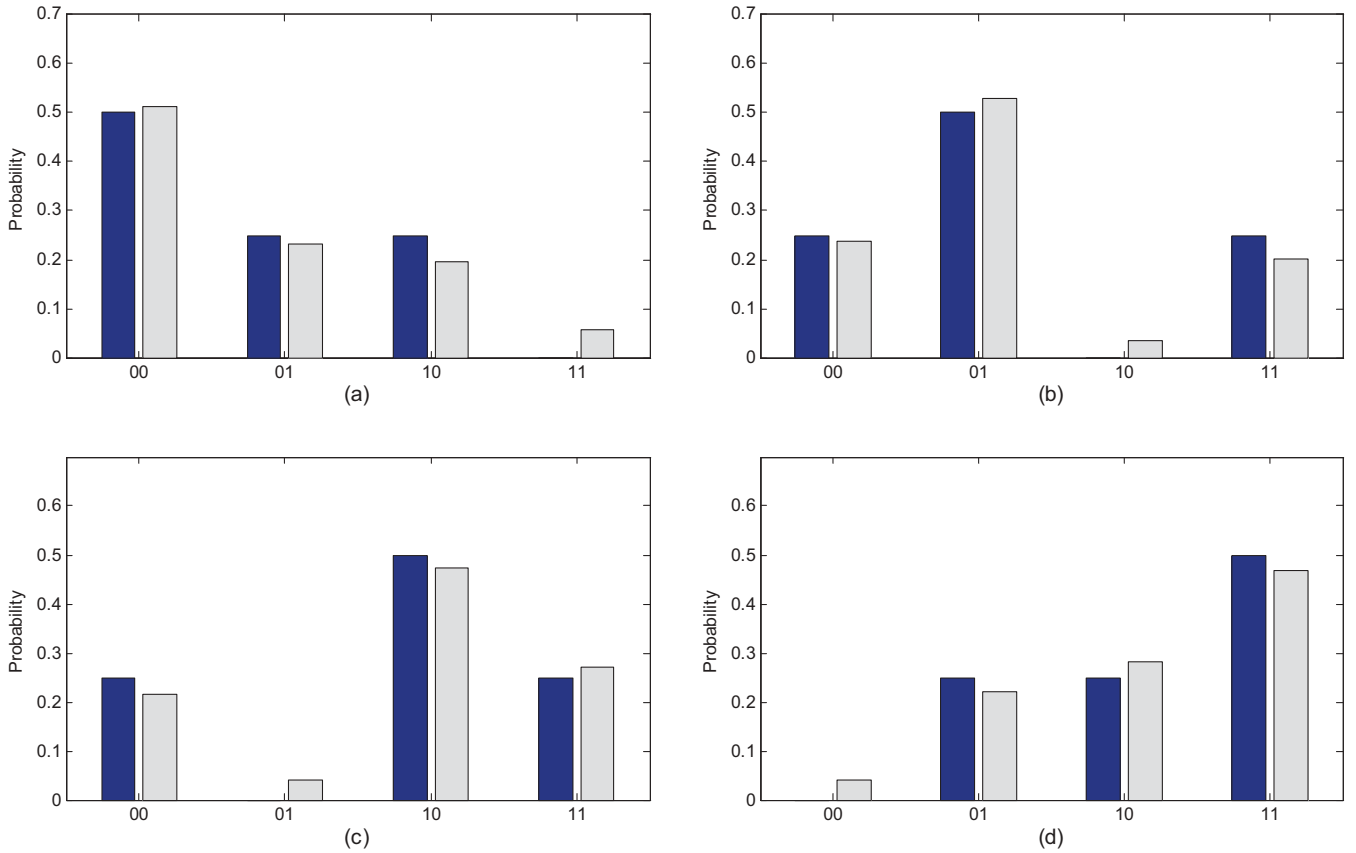

FIG. 5. (Color online) Experimental results of the SKW algorithm. Parts (a)–(d) correspond to the cases of finding $|00\rangle_{12}$, $|01\rangle_{12}$, $|10\rangle_{12}$, and $|11\rangle_{12}$, respectively. The blue (dark) bars represent the theoretical prediction and the gray (light) bars represent the experimental analog, respectively.

calculated. Now we have accomplished the diagonal elements' tomography.

C. Experiment

The experiment was divided into three steps: the pseudo-pure-state preparation, quantum-random-walk searching process, and population measurement. Starting from the thermal equilibrium state, first we need to create the PPS $\rho_{000} = \frac{1-\epsilon}{8}\mathbf{1} + \epsilon|000\rangle\langle 000|$, where ϵ represents the polarization of the system and $\mathbf{1}$ is the identity matrix. We used strongly modulating pulses based on the gradient ascent pulse engineering (GRAPE) algorithm [27–29] and gradient pulses to realize the PPS preparation, with a numerical simulated fidelity of 0.977. The top spectrum of Fig. 4 shows the experimental observation of the PPS about the first qubit in the eigenbasis, which exhibits a single absorption-shape peak if the small errors are discarded.

The quantum-random-walk searching process actually contains two parts: the preparation of the initial state $|+\rangle^{\otimes 3}$ ($|+\rangle = (|0\rangle + |1\rangle)/\sqrt{2}$) and two iterations of unitary evolution. We packed them together and calculated one GRAPE pulse of 20 ms and 250 segments whose fidelity is higher than 0.990. The reading-out operators listed in Table II are also performed when generating the GRAPE pulses of 20 ms with fidelity 0.990. Four spectra observed on transition 9 (marked by the ellipse) are shown in Fig. 4. The results are extracted from the spectra through integration of NMR peaks referenced by the PPS spectrum. The fidelity of the diagonal elements of the final density matrix is 0.983, with the probabilities of gaining $|00\rangle$, $|01\rangle$, $|10\rangle$, and $|11\rangle$ being 0.513, 0.232, 0.197, and 0.058, respectively. It demonstrates that we have completed searching $|00\rangle$ based on the SKW algorithm.

Besides $|00\rangle$, we altered the target states to $|01\rangle$, $|10\rangle$, and $|11\rangle$. The experimental results of the SKW algorithm are plotted in Fig. 5. It can be seen that the experimental and theoretical results are mostly consistent, with little error. The slight difference between theory and experiment may be attributed to decoherence, the rf field inhomogeneity, and imperfect implementation of GRAPE pulses. In order to judge the credibility of the experimental spectra, the simulated spectra are shown in Fig. 4 using the NMR-sim software of Topspin. Given the Hamiltonian, GRAPE pulses, and pulse sequence, the software can show the simulated spectra without the experimental imperfections. The minor difference in linewidth is caused mainly by the slightly different time (T_2) used in the simulation. Within the acceptable error range, the simulated and experimental linewidths are consistent.

IV. CONCLUSION

In summary, we experimentally implemented a search algorithm based on the quantum random walk (the SKW algorithm) in the case of 1 out of 4. This algorithm performs an oracle search on a database of N items with $O(\sqrt{phN})$ calls, with a speedup similar to the Grover search algorithm. The experiment was carried out on an NMR quantum information processor with strongly dipolar coupled spins. We used GRAPE pulses to realize high-fidelity unitary operations and provided an effective way to measure the diagonal elements of the density matrix with one-dimensional NMR spectra. The experimental results agree well with the theoretical expectations, which exhibits the superiority of the algorithm.

This method is going to be extended to full tomography and higher qubits. For further high qubits, the process becomes very challenging due to the complexity in the calculation of GRAPE pulses and diagonalization of the Hamiltonian. However, as the speed and power of computers and schemes of calculation advance, these obstacles may be alleviated considerably in the near future. Therefore, this method, as in the case of low qubits, may still be a useful and effective method to test many interesting quantum algorithms and quantum-information tasks.

ACKNOWLEDGMENTS

We thank Dieter Suter and Yiheng Lin for their help. This work was supported by the National Nature Science Foundation of China under Grant No. 10975124, Ministry of Education of PRC, Chinese Academy of Sciences, National Fundamental Research Program 2007CB925200.

[1] P. W. Shor, SIAM J. Comput. **26**, 1484 (1997).
[2] L. K. Grover, Phys. Rev. Lett. **79**, 325 (1997).
[3] E. Farhi, J. Goldstone, S. Gutmann, J. Lapan, A. Lundgren, and D. Preda, Science **292**, 472 (2001).
[4] Y. Aharonov, L. Davidovich, and N. Zagury, Phys. Rev. A **48**, 1687 (1993).
[5] E. Farhi and S. Gutmann, Phys. Rev. A **58**, 915 (1998).
[6] A. Ambainis, E. Back, A. Nayak, A. Vishwanath, and J. Watrous, in *Proceedings of the 30th Annual ACM Symposium on Theory of Computing* (Association for Computing Machinery, New York, 2001), pp. 60–69.
[7] A. Childs, E. Farhi, and S. Gutmann, Quant. Info. Proc. **1**, 35 (2002).
[8] A. Childs, R. Cleve, E. Deotto, E. Farhi, S. Gutmann, and D. Spielman, in *Proceedings of the 35th ACM Symposium on Theory of Computing* (STOC 2003), pp. 59–68.
[9] T. A. Brun, H. A. Carteret and A. Ambainis, Phys. Rev. Lett. **91**, 130602 (2003).
[10] A. Ambainis, SIAM J. Comput. **37**, 210 (2007).
[11] E. Farhi, J. Goldstone, and S. Gutmann, Theory Comput. **4**, 169 (2008).
[12] A. M. Childs, Phys. Rev. Lett. **102**, 180501 (2009).
[13] N. Shenvi, J. Kempe, and K. Birgitta Whaley, Phys. Rev. A **67**, 052307 (2003).
[14] A. Ambainis, J. Kempe, and A. Rivosh, in *Proceedings of the 16th ACM-SIAM SODA* (Society for Industrial and Applied Mathematics, Philadelphia, 2005), pp. 1099–1108.
[15] A. Tulsi, Phys. Rev. A **78**, 012310 (2008).
[16] D. Reitzner, M. Hillery, E. Feldman, and V. Buzek, Phys. Rev. A **79**, 012323 (2009).
[17] C. M. Chandrashekar, R. Srikanth, and R. Laflamme, Phys. Rev. A **77**, 032326 (2008).

[18] V. Potoček, A. Gábris, T. Kiss, and I. Jex, Phys. Rev. A **79**, 012325 (2009).
[19] B. C. Travaglione and G. J. Milburn, Phys. Rev. A **65**, 032310 (2002).
[20] J. Du, H. Li, X. Xu, M. Shi, J. Wu, X. Zhou, and R. Han, Phys. Rev. A **67**, 042316 (2003).
[21] C. A. Ryan, M. Laforest, J. C. Boileau, and R. Laflamme, Phys. Rev. A **72**, 062317 (2005).
[22] C. M. Chandrashekar, Phys. Rev. A **74**, 032307 (2006).
[23] T. S. Mahesh and D. Suter, Phys. Rev. A **74**, 062312 (2006).
[24] M. K. Henry, C. Ramanathan, J. S. Hodges, C. A. Ryan, M. J. Ditty, R. Laflamme, and D. G. Cory, Phys. Rev. Lett. **99**, 220501 (2007).
[25] J. Zhang, M. Ditty, D. Burgarth, C. A. Ryan, C. M. Chandrashekar, M. Laforest, O. Moussa, J. Baugh, and R. Laflamme, Phys. Rev. A **80**, 012316 (2009).
[26] N. Suryaprakash, Curr. Org. Chem. **4**, 85 (2000).
[27] N. Khaneja *et al.*, J. Magn. Reson. Im. **172**, 296 (2005).
[28] J. Baugh *et al.*, Phys. Can. **63**, 22 (2007).
[29] C. A. Ryan, C. Negrevergne, M. Laforest, E. Knill, and R. Laflamme, Phys. Rev. A **78**, 012328 (2008).